(Preprint) IAA-AAS-DyCoSS1 -14-07

ANALYSIS OF INTERPLANETARY SOLAR SAIL TRAJECTORIES WITH ATTITUDE DYNAMICS

Andreas Borggräfe[*], Andreas Ohndorf[†], Bernd Dachwald[‡], Wolfgang Seboldt[§]

We present a new approach to the problem of optimal control of solar sails for low-thrust trajectory optimization. The objective was to find the required control torque magnitudes in order to steer a solar sail in interplanetary space. A new steering strategy, controlling the solar sail with generic torques applied about the spacecraft body axes, is integrated into the existing low-thrust trajectory optimization software *InTrance*. This software combines artificial neural networks and evolutionary algorithms to find steering strategies close to the global optimum without an initial guess. Furthermore, we implement a three rotational degree-of-freedom rigid-body attitude dynamics model to represent the solar sail in space. Two interplanetary transfers to Mars and Neptune are chosen to represent typical future solar sail mission scenarios. The results found with the new steering strategy are compared to the existing reference trajectories without attitude dynamics. The resulting control torques required to accomplish the missions are investigated, as they pose the primary requirements to a real on-board attitude control system.

INTRODUCTION

Solar sails have been investigated in the literature as an alternative to other low-thrust propulsion concepts for interplanetary space exploration missions, since they produce the required thrust by momentum exchange with the solar photonic flux and do not require any propellant. They enable flexible, high-ΔV missions with mission times limited only by the integrity of the thin sail membrane, the lifetime of the onboard subsystems and the distance from the Sun. Solar sails consist of large and ultra-lightweight reflective membranes deployed by a flexible supporting boom structure, resulting in large mass moments of inertia. Consequently, attitude changes of solar sails are generally slow and delayed, demanding a sophisticated steering strategy. Future mission scenarios for solar sails most likely require a variety of control torque magnitudes, depending on the physical dimensions of the sail and on the expected steering maneuvers along the transfer trajectory. Accordingly, we chose two interplanetary mission scenarios that represent possible lower and upper boundaries of the expected control torque demands, a Mars rendezvous and a Neptune flyby. The latter requires multiple solar photonic assist (SPA) maneuvers close to the Sun (< 0.3 AU) in order to gain enough kinetic energy to reach Neptune in a reasonable time-of-flight (TOF).[1] These maneuvers are very ambitious with regard to sail attitude changes. Mars is a very common scenario for solar sail performance analysis and demands moderate steering requirements, since its orbit is

[*]Postgraduate Student, Advanced Space Concepts Laboratory, Department of Mechanical and Aerospace Engineering, University of Strathclyde, Glasgow, United Kingdom, andreas.borggraefe@strath.ac.uk
[†]Project Manager, German Aerospace Center (DLR), Oberpfaffenhofen, Germany, andreas.ohndorf@dlr.de
[‡]Professor, FH Aachen University of Applied Sciences, Aachen, Germany, dachwald@fh-aachen.de
[§]Senior Scientist, German Aerospace Center (DLR), Köln, Germany, wolfgang.seboldt@dlr.de

the closest to Earth in outbound direction and has a relatively small inclination of 1.85 deg. Even near-term sail technologies are able to reach Mars within 2-3 years. A 160-m, 450-kg square solar sail was used throughout this study with a nominal solar thrust force of 160 mN (at 1 AU).[2] The time-optimal trajectories for both missions are calculated using the low-thrust trajectory optimization software *InTrance*[*]. The software combines Artificial Neural Networks (ANN) and Evolutionary Algorithms (EA) to find steering strategies close to the global optimum without an initial guess.[3] Based on optimal control theory, trajectory optimization algorithms for low-thrust propulsion missions typically calculate the local optimal thrust-vector direction for each time-step. During the simulation, the local thrust direction and hereby the attitude of the solar sail is changed instantaneously into the desired direction. This existing approach was termed 'instant thrust vector steering' (ITS) strategy throughout this study. It significantly idealizes the real in-space flight physics of the spacecraft, since the rotational inertia of the sail are not included. The equations of motion for solar sails that are incorporated in the optimization software therefore account only for the three translational degree-of-freedom (DOF). Within the implemented new attitude dynamics model, we expand the spacecraft's state vector using a quaternion-based three DOF attitude representation of the solar sail and the corresponding rate of change. We derived the governing equations of rotational motion in quaternion form, resulting in a differential equation system of first order. Within the attitude dynamics model, the solar sail membrane is assumed as a rigid body, not accounting for any billowing, vibrational or wrinkling effects. The ANN in InTrance is modified to find the control torques necessary to rotate the sail into the local optimal flight attitude. Within the scope of this work, generic control torques are assumed and no physical AOCS[†] is simulated. This new 'control torque steering' (CTS) strategy is intended to search for the locally optimal control torques that change the sail attitude and likewise its solar radiation pressure (SRP) force vector $\boldsymbol{F}_{\mathrm{SRP}}$ into the optimal direction. For all trajectory calculations, the so-called 'simple sail force model' is used, which assumes a perfectly reflecting sail membrane and a resulting $\boldsymbol{F}_{\mathrm{SRP}}$ vector perpendicular to the sail surface. For all calculations, a RUNGE-KUTTA-FEHLBERG method of order 4(5) is used for numerical integration of the translational and rotational EOM.

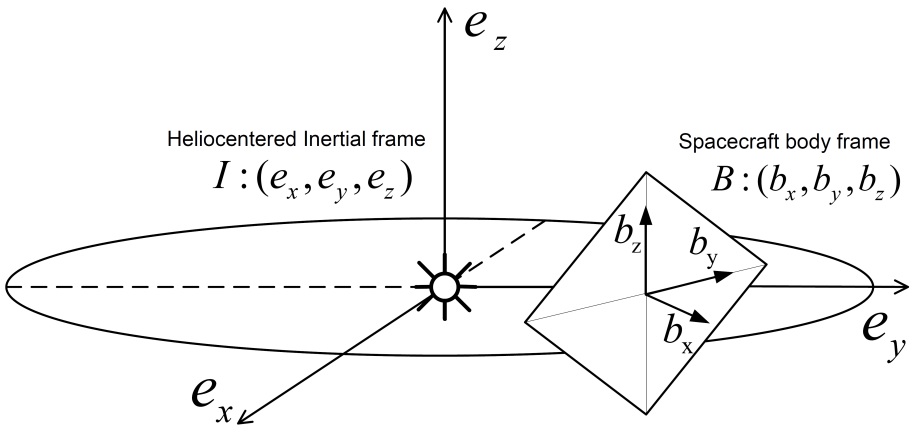

Figure 1: Body-fixed frame $\mathcal{B}$ and inertial heliocentered reference frame $\mathcal{I}$

[*]"Intelligent Trajectory optimization using neurocontroller evolution" (Bernd Dachwald, Andreas Ohndorf, DLR)
[†]Attitude and Orbit Control System

PRINCIPLES OF SOLAR SAILING

A solar sail utilizes the solar radiation pressure (SRP) of the photons emitted by the Sun. By impinging on a large, very thin (a few μm) reflective surface, the momentum of the solar photonic flux is transferred to the sail and applies a force that accelerates the spacecraft. The resulting SRP force vector $\boldsymbol{F}_{\text{SRP}}$ is approximately perpendicular to the sail surface and always directed away from the Sun. In reality, $\boldsymbol{F}_{\text{SRP}}$ is slightly deflected from the sail normal due to the non-ideal properties of the sail membrane. The SRP force vector direction and magnitude is described in the literature by several mathematical SRP force models.[4] They are derived both from an analytical perspective and from empirical and/or experimental investigations. The models describe the resulting SRP forces acting on a solar sail as a function of the primary variables Sun distance, light incidence angle and optical sail surface properties. Within the widely used 'simple solar sail force model', the sail surface is simplified as a perfect reflector and no material properties are included in this model. The SRP force vector direction is described by the sail normal vector $\boldsymbol{n}$, the unit vector perpendicular to the sail surface and always directed away from the Sun ($\boldsymbol{n} \cdot \boldsymbol{e}_r \geq 0$). However, its direction does not entirely define the sail's attitude in terms of all three degrees of (rotational) freedom, since the rotation angle ϕ_n about the vector $\boldsymbol{n}$ is arbitrary. Nevertheless, it is sufficient to quantify the SRP force magnitude, because the projected sail area $A_{\text{proj}} = A \cdot (\boldsymbol{n} \cdot \boldsymbol{e}_r)$ is the same for all ϕ_n. The direction of $\boldsymbol{n}$ is conveniently described by the sail cone angle α and the sail clock angle δ, according to Figure 2. Both angles are defined in the spacecraft-centered osculating* orbit reference frame $\mathcal{O} : (\boldsymbol{e}_r, \boldsymbol{e}_t, \boldsymbol{e}_h)$ (see Appendix B). The clock angle δ is measured between the $\boldsymbol{e}_t$-axis and the projection of the sail normal direction $\boldsymbol{n}$ in the $(\boldsymbol{e}_t, \boldsymbol{e}_h)$-plane. The cone angle α is located between the $\boldsymbol{e}_r$-axis and the sail normal direction $\boldsymbol{n}$.

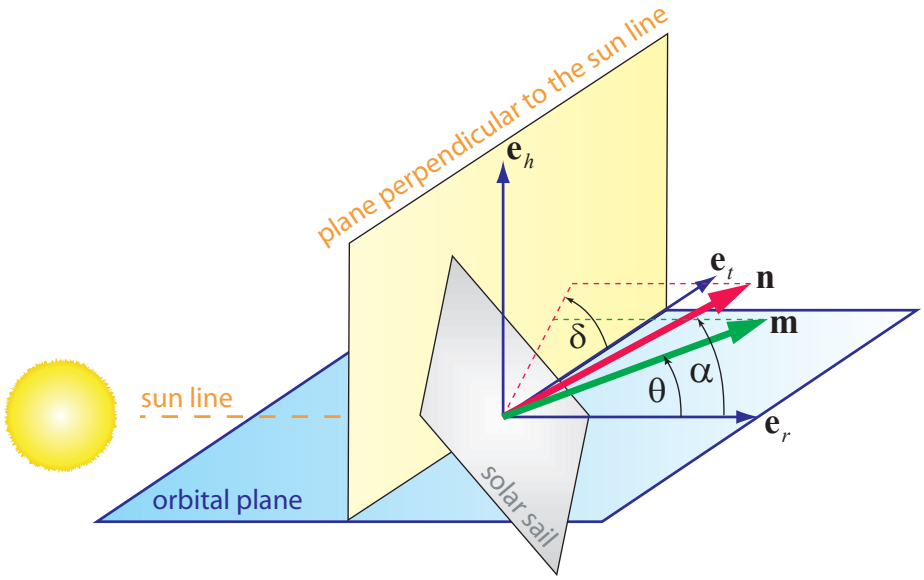

Figure 2: Solar sail steering angles α and δ and sail normal vector $\boldsymbol{n}$ in orbit reference frame $O : (\boldsymbol{e}_r, \boldsymbol{e}_t, \boldsymbol{e}_h)$

*instantaneous orbital elements that would be obtained without thrust and only gravitation of a perfectly sphere-shaped central body was acting on the spacecraft

For the simple sail force model, it can be shown that the total SRP force exerted on the sail surface results as

$$\boldsymbol{F}_{\text{SRP}} = 2\eta A P_0 \Big(\frac{r_0}{r}\Big)^2 \cos^2\alpha\, \boldsymbol{n} \tag{1}$$

with the SRP at 1 AU distance from the Sun $P_0 = 4.563\ \mu\text{N/m}^2$. As visible from Equation 1, the accelerating force depends only on the sail cone angle α and not on the sail clock angle δ, since a change in δ does not change the projected sail area $A_{\text{proj}} = A \cdot \cos\alpha$ towards the sun. Throughout solar sail-related literature, a sail efficiency factor η is widely used within the simple force model to allow for the non-perfect optical properties of the sail surface and billowing of the sail film under load.[4] Typical values of η are between 0.85 and 0.9. However, this factor is not based on any empirical data. In the presented mission analysis, we use the simple SRP force model exclusively, since it provides a sail thrust vector in sail normal direction ($\boldsymbol{F}_{\text{SRP}} = \boldsymbol{n}$). This is beneficial in the course of analyzing the effects of sail attitude on the selected mission scenarios, since no deflection of the force direction must be accounted for. The error in simulation accuracy relative to the other existing SRP force models[5] is negligible for preliminary mission analysis. The following solar sail performance parameter are usually used in the literature. The characteristic acceleration a_c is defined as the SRP acceleration acting on a sail oriented perpendicular to the Sun-sail line ($\boldsymbol{n} \cdot \boldsymbol{e}_r = 1$, $\alpha = 0$ deg) at Sun-Earth distance $r_0 = 1$ AU. According to Equation 1, the characteristic acceleration for the simple model results as $a_{c,\text{simple}} = 2\,\eta\,P_0\,A/m$. The lightness number β is defined as the ratio of the sail's SRP acceleration $a_{\text{SRP}}(r) = a_c(r_0/r)^2$ and the solar gravitational acceleration $a_{\text{G}}(r) = \mu_{\text{S}}/r^2$. The Sun's gravitational acceleration at Earth distance is $a_0 = a_{\text{G}}(r_0) = \mu_{\text{S}}/r_0^2 = 5.930\ \text{mm/s}^2$. The lightness number is now defined as $\beta = a_{\text{SRP}}(r)/a_{\text{G}}(r) = a_c\, r_0^2/\mu_{\text{S}} = a_c/a_0$. Since both accelerations are proportional to $1/r^2$, the lightness number is independent of the Sun-sail distance.

Translational Equations of Motion for Solar Sails

The equations of heliocentric translational motion for solar sails are implemented in *InTrance* and used to calculate the sail's motion in interplanetary space. Generally, the motion of a spacecraft is determined by gravitational forces of the celestial bodies (the Sun, planets, moons and minor bodies), 'perturbative' forces of non-spherical gravitational fields, solar wind, possibly atmospheric drag (and lift) near planetary atmospheres and the spacecraft SRP force. The 'translational equations of motion' (TEOM) for the ideal SRP force model, resolved along the unit vectors of the ecliptic reference frame $\mathcal{E}$ (see Appendix A) in terms of radial r, azimuth φ and elevation θ components, are given below[3]

$$\ddot{r} = r\dot{\theta}^2 + r\dot{\varphi}^2\cos^2\theta - \frac{\mu}{r^2} + \lambda\frac{\mu}{r^2}u_1 \tag{2a}$$

$$\ddot{\varphi} = -2\frac{\dot{r}\dot{\varphi}}{r} + 2\dot{\varphi}\dot{\theta}\tan\theta + \lambda\frac{\mu}{r^2}\frac{u_2}{r\cos\theta} \tag{2b}$$

$$\ddot{\theta} = -2\frac{\dot{r}\dot{\theta}}{r} - \dot{\varphi}^2\sin\theta\cos\theta + \lambda\frac{\mu}{r^2}\frac{u_3}{r} \tag{2c}$$

Here, the control functions u_1, u_2 and u_3 represent the $\boldsymbol{F}_{\text{SRP}}$ components and thus depend on the sail angles α, δ and the orbit angle ζ between the polar ecliptic frame $\mathcal{E}$ and the orbit frame $\mathcal{O}$ (see Appendix B)

$$u_1(\alpha) = \cos^3 \alpha \tag{3a}$$

$$u_2(\delta + \zeta, \alpha) = \cos(\delta + \zeta) \sin \alpha \cos^2 \alpha \tag{3b}$$

$$u_3(\delta + \zeta, \alpha) = \sin(\delta + \zeta) \sin \alpha \cos^2 \alpha \tag{3c}$$

The control functions u_1, u_2 and u_3 are the components of the spacecraft control vector $\boldsymbol{u}(t_i)$ that is (using some transformations) calculated by the steering neurocontroller (NC) in *InTrance* for each time-step t_i during the trajectory optimization (see below). Within the present ITS strategy used in *InTrance*, the neurocontroller calculates the u_i-components directly, commanding a respective SRP force vector direction. Within the new implemented CTS strategy, the u_i-components are not provided by the NC anymore. The NC is modified to return the three control-torque components T_i about the spacecraft body axes and the sail rotates according to the rotational equations of motion (see next paragraph). In parallel, the new direction of the sail control vector $\boldsymbol{u}(t_i)$ is calculated from the new sail attitude and then used within the coupled TEOM.

Rotational Equations of Motion for Solar Sails

The equations of rotational motion (REOM) are derived from EULERs equation, assuming the solar sail as a rigid body. The REOM are parameterized in quaternion form*, $\ddot{\bar{q}} = f(\bar{q}, \dot{\bar{q}}, \boldsymbol{T}, [I], \boldsymbol{\omega})$, describing the second derivative of the attitude quaternion $\ddot{\bar{q}}$ due to external control torques $\boldsymbol{T}$ about the three principal body axes.[5] The quaternion $\bar{q}$ expresses the solar sail body frame $\mathcal{B}$ attitude relative to the heliocentered inertial frame $\mathcal{I}$. $\mathcal{B}$ is chosen to be a principal axes frame.† According to the above assumptions, the sails mass moments of inertia tensor $[I]$ is diagonal, constant and no products of inertia terms appear. $\ddot{\bar{q}}$ is further a function of the rate of change of this attitude $\dot{\bar{q}}$ and the sail's angular velocity $\boldsymbol{\omega}$, using the so-called 'quaternion product' operator '$\otimes$' (see Appendic C). The resulting differential equation system of rotational motion of a rigid body can be written as

$$\ddot{\bar{q}} = \dot{\bar{q}} \otimes \bar{q}^{-1} \otimes \dot{\bar{q}} + \frac{1}{2}\, \bar{q} \otimes \dot{\bar{\omega}} \qquad \text{with } \dot{\bar{\omega}} = \begin{pmatrix} [I]^{-1}(\boldsymbol{T} - \boldsymbol{\omega} \times [I]\boldsymbol{\omega}) \\ 0 \end{pmatrix} \tag{4}$$

CAPABILITIES AND CONSTRAINTS OF SOLAR SAILS

Other low-thrust spacecraft can point their thrust vector in any desired direction, but the thrust vector $\boldsymbol{F}_{\text{SRP}}$ of a solar sail is constrained to lie on the surface of a 'bubble' that is always directed away from the Sun, Figure 3. Indeed, by adjusting the solar sail attitude relative to the Sun, the sail either produces a positive (in flight direction) or negative (against flight direction) orbit-transversal acceleration component $\boldsymbol{a}_t$. Accordingly, the sail gains orbit energy and spirals outwards (away from the Sun) or loses orbit energy, spiraling inwards (towards the Sun), which enables a wide

*a four-dimensional quaternion vector is marked with an upper '-' to distinguish it from other algebraic elements

†a coordinate frame aligned with a bodies' principal axes of inertia

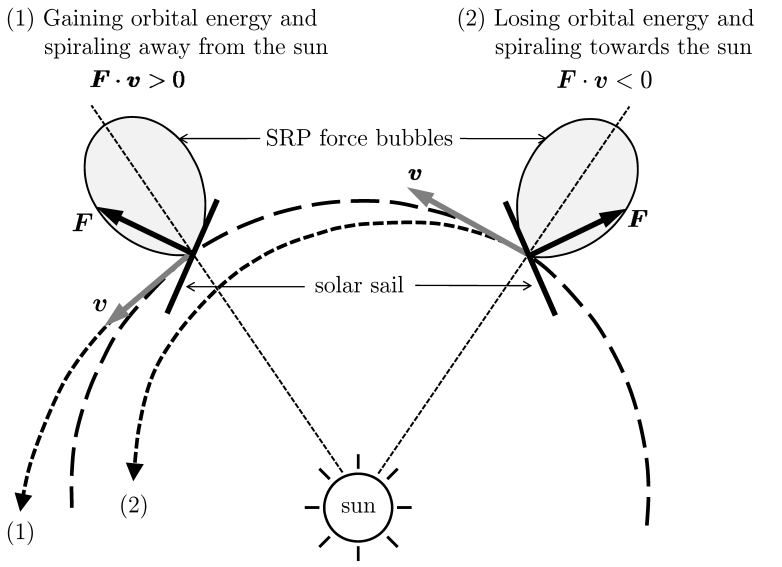

Figure 3: SRP force vector $\boldsymbol{F}_{\text{SRP}}$-bubble and spiraling of the solar sail

range of mission applications. As seen in the simple solar sail force model, Equation 1, the SRP force magnitude $|\boldsymbol{F}_{\text{SRP}}|$ is coupled to the force direction, restricting the maneuverability of the sail in comparison to other low-thrust propulsion systems. As can be shown from the SRP force models, the solar sail provides its maximum transversal force component for cone angles $\alpha \approx 35$ deg. The radial acceleration component a_r reaches its maximum at 0 deg. As will be seen in later mission analysis, the sail will mainly use these extremal angles during the investigated missions. When directing a fraction of the SRP force vector $\boldsymbol{F}_{\text{SRP}}$ out of the orbit plane (thus $\alpha \neq 0$), the inclination of the osculating orbit can also be changed due to a sail acceleration component a_h normal to the orbit plane. This enables missions like observation of the Sun's polar regions or rendezvous with highly inclined small solar system bodies. By flying close to the Sun, the solar sail is able to gain the kinetic energy to reach a hyperbolic trajectory and thus to realize even fast solar system escape missions.[6] Therefore, the sail must accomplish one or several so called Solar Photonic Assist Maneuver (SPA). This maneuver characterizes a close flyby at the Sun with an orbit perihelion $r_p < 0.3$ AU.[1] SPAs enable a solar sail to reach the outer planets and the edge of the solar system. On the other hand, without additional thrusters for braking at the target body or aerocapture maneuvers, only fast fly-by missions are possible.

Knowing the highest possible SRP force in orbit-radial and transversal direction is insufficient for the evaluation of the orbit dynamics of a solar sail. It is also important to know the preferable direction of the SRP force in order to accomplish a designated space mission in an optimal way, e.g., in minimum time. During an interplanetary mission, the optimal transfer trajectory requires an optimal change of one (or several) KEPLERian orbital elements (a, e, ι, Ω, f). This can be seen through LAGRANGE's variational equations.[7] These equations provide a connection between the change of an orbital element as a result of the applied force (gravitational, perturbing or propulsive). As visible from the equations, it is not possible to affect only one orbital element at a time. Moreover, only forces within the orbital plane change the semi-major axis a and the eccentricity e of the orbit. An arbitrary force, neither in the orbit plane nor perpendicular to it, changes all orbital elements at the same time. Hence, some elements may be changed unintendedly, while trying to optimize another.

These circumstances show the complexity of the low-thrust optimization problem.[3] Although these equations are very complex in nature, some simplified correlations can be found. First, in order to change the orbit energy (semi-major axis a) with a maximum rate, the sail's transversal acceleration component $\boldsymbol{a}_t$ needs to be maximized (to reach for example Mars or Venus). Second, for a maximum change of the orbit's eccentricity e, the sail radial acceleration component $\boldsymbol{a}_r$ must obtain a maximum, e.g. to reach a highly eccentric orbit of a comet/asteroid.

TRAJECTORY OPTIMIZATION AND EVOLUTIONARY NEUROCONTROL

Within this paper, evolutionary neurocontrol (ENC) is used to calculate optimal (time-minimal) solar sail trajectories. This method is based on a combination of artificial neural networks (ANNs) and evolutionary algorithms (EAs). ENC tackles low-thrust trajectory optimization problems from the perspective of artificial intelligence and machine learning. Here, it can only be sketched how this method is used to search for optimal solar sail trajectories. The reader who is interested in the details of the method is referred to the reference.[3,8] The problem of searching an optimal solar sail trajectory $\boldsymbol{x}^*(t) = (\boldsymbol{r}^*(t), \dot{\boldsymbol{r}}^*(t))^*$ is equivalent to the problem of searching an optimal sail force vector history $\boldsymbol{F}^*_{\mathrm{SRP}}(t)$, which is defined by the optimal time history of the spacecraft control vector $\boldsymbol{u}^*(t)$. Within the context of machine learning, a trajectory is regarded as the result of a steering strategy S that maps the problem relevant variables (the astrodynamic spacecraft state $\boldsymbol{x}$ and the target-body state $\boldsymbol{x}_T$) onto the control vector, $S : \boldsymbol{x}, \boldsymbol{x}_T \in R^{12} \mapsto \boldsymbol{u} \in \mathcal{R}^3$, which is used within the TEOM to integrate the trajectory. This way, the problem of searching $\boldsymbol{x}^*(t)$ is equivalent to the problem of searching (or learning) the optimal steering strategy S^*. An ANN is used as a NC to implement solar sail steering strategies. It can be regarded as a parameterized network function N_π that is - for a fixed network topology - completely defined by the internal parameter set π of the ANN. Therefore, each π_i defines a sail steering strategy S_{π_i}. The problem of searching $\boldsymbol{x}^*(t)$ is therefore equivalent to the problem of searching the optimal NC parameter set π^*. EAs that work on a population of strings are used for finding π^*, because π can be mapped onto a string ξ (also called chromosome or individual). The trajectory optimization problem is solved when the optimal chromosome ξ^* is found. Evolutionary neurocontrol (ENC) is a NC that employs an EA for learning (or breeding) π^*. ENC was implemented within a low-thrust trajectory optimization program called *InTrance*, which stands for Intelligent Trajectory optimization using neurocontroller evolution. *InTrance* is a smart global trajectory optimization method that requires only the initial spacecraft and target-body state as input to find a trajectory close to the global optimum for the specified problem. It works without an initial guess and does not require the attendance of a trajectory optimization expert during the optimization run.

The necessary adaptions to the NC that steers the solar sail according to the new CTS strategy are presented below. Since the NC no longer returns the local optimal spacecraft control vector $\boldsymbol{u}^*(t_i)$ but the local optimal control torques $\boldsymbol{T}^*(t_i)$ about the three body axes, several changes to *InTrance* were necessary. Most important are the changes to the network's input parameters, according to the new optimization problem. The NC receives information about the current spacecraft body and target states for each control step and steers the spacecraft according to the current chromosome parameterization ξ_i, which determines the steering strategy S_{π_i}. The NC input parameters are essential for the NC's steering capability. Within the existing ITS strategy in *InTrance*, the NC receives up to 18 different parameters[†] like the state variables $\boldsymbol{r}(t), \dot{\boldsymbol{r}}(t)$ of the spacecraft, the target distance

[*] the variable t denotes the time history and the symbol $*$ denotes the optimal value

[†] depending on the chosen trajectory optimization problem

$|\boldsymbol{x}_{\text{SC}} - \boldsymbol{x}_{\text{t}}|$ and its rate of change. With the new CTS strategy, a set of new NC input parameters become accessory. These are the sail attitude $\bar{q}(t_i)$ and the sail angular velocity $\boldsymbol{\omega}(t_i)$ with respect to the inertial frame $\mathcal{I}$. A set of new functionalities are enabled alongside with the attitude dynamics model. The initial sail attitude can be configured w.r.t. $\mathcal{I}$- or $\mathcal{E}$-frame and the solar sail's initial angular velocity $\boldsymbol{\omega}_{\text{init}}$ can be configured about all body axes $\mathcal{B} = (\boldsymbol{b}_x, \boldsymbol{b}_y, \boldsymbol{b}_z)^T$.

In order to optimize the search for an optimal solution, a set of abort criteria are added to the trajectory optimization process. They are implemented as simulation constraints, forcing the integrator to stop the trajectory propagation when the constraint is reached. The respective steering strategy S_{π_i} receives a highly negative fitness value J_{π_i} from the EA. This procedure force all corresponding S_{π_i} to eventually die out of the population. For example, the sail cone angle α can be limited to avoid attitudes with the sail's back-side towards the Sun. Obtaining this attitude, the sail would produce no SRP force, because the back-side surface is made of chromium and has no appropriate optical properties. In fact, it is optimized for maximum thermal radiation and thus supports to keep the sail below its maximum allowed temperature. Subjecting its back-side to the Sun, the solar sail is most likely to be destroyed. Likewise, the sail's maximum allowed angular velocity $\boldsymbol{\omega}_{\text{max}}$ can be configured. This should avoid uncontrolled tumbling of the sail, as observed in an early validation campaign. In addition, a dynamic step size control is embedded depending on the sail's angular velocity.

SOLAR SAIL CONFIGURATION

The solar sail used throughout this study was taken from the 160-m, 450-kg Solar Polar Imager (SPI) sail configuration proposed by Wie in 2006.[2,9]

Table 1: Solar sail specifications of 160-m, 450-kg SPI (Solar Polar Imager) mission, taken from[2]

sail area	$A = a \cdot b$	$(160\text{ m})^2 = 25600\ [\text{m}^2]$
scallop (billowing) factor	η_{s}	0.75
effective sail area	$A_{\text{eff}} = \eta_{\text{s}} \cdot A$	$(138.5\text{ m})^2 = 19200\ [\text{m}^2]$
sail assembly mass	m_{SA}	150 [kg]
spacecraft bus mass	m_{Bus}	250 [kg] (approx. as point mass)
payload mass	m_{PL}	50 [kg] (approx. as point mass)
total mass	m_{total}	450 [kg]
effective sail loading	$\sigma_{\text{eff}} = m_{\text{total}}/A_{\text{eff}}$	$23.44\ [\text{g/m}^2]$
sail efficiency factor (for simple model)	η	0.84
eff. char. acceleration (simple model)	$a_{\text{c,simple}}$	$0.33\ [\text{mm/s}^2]$
lightness number (simple model)	β_{simple}	0.056
mass moments of inertia		
about body x-axis	I_{b_x}	640,000 [kg m^2]
about body y- and z-axis	$I_{\text{b}_\text{y}} = I_{\text{b}_\text{z}}$	320,000 [kg m^2]

The sail parameters are shown in Table 1, bold values are calculated in addition. The total sail mass is subdivided into the sail assembly mass* $m_{\text{SA}} = 150$ kg, the payload mass $m_{\text{PL}} = 50$ kg and the spacecraft bus mass $m_{\text{Bus}} = 250$ kg. The mass moments of inertia along the three principal

*containing the mass of the sail membrane and the required structure for storing, deploying and tensioning of the sail

body axes are calculated assuming the spacecraft bus and payload as point masses in the center of mass (CoM), without inertia. Accordingly, the relevant mass for the I-terms is $m_{\mathrm{SA}} = 150$ kg. We calculate $I_{\mathrm{b_x}} = m_{\mathrm{SA}}(a^2 + b^2)/12 = m_{\mathrm{SA}}A/6$ and $I_{\mathrm{b_y}} = I_{\mathrm{b_z}} = m_{\mathrm{SA}}b^2/12 = m_{\mathrm{SA}}A/12$, based on a solid cuboid with zero depth due to the negligible thickness of the sail membrane. Since the sail is no ideal flat plate but will billow under load, a scallop (billowing) factor of $\eta_{\mathrm{s}} = 0.75$ for the projected sail area was used in the reference. Accordingly, the effective sail area for calculating the SRP force reduces to $A_{\mathrm{eff}} = \eta_{\mathrm{s}} \cdot A = 19200\ \mathrm{m}^2$. Using the simple sail force model and employing a sail efficiency factor $\eta = 0.84$ to allow for the non-perfect optical properties of the sail membrane, the sail's characteristic acceleration is $a_{\mathrm{c,simpl}} = 2\eta\eta_{\mathrm{s}}P_0A/m = 0.33\,\mathrm{mm/s^2}$. The corresponding lightness number is $\beta_{\mathrm{simple}} = 0.056$.

MISSION ANALYSIS

An interplanetary body rendezvous mission between Earth and Mars is chosen as a first scenario for the comparison of the new CTS strategy with the existing ITS strategy. The Mars orbit parameters are semi-major axis $a_{\mathrm{M}} = 1.5237$ AU, eccentricity $e_{\mathrm{M}} = 0.0934$ and inclination $\iota_{\mathrm{M}} = 1.85$ deg. Starting from Earth, the initial orbit conditions are $a_{\mathrm{E}} = 1.0$ AU, $e_{\mathrm{E}} = 0.0167$ and $\iota_{\mathrm{E}} = 0$ deg. The time-minimal transfer trajectory requires an optimal change in one (or several) orbital elements, as can be seen through the LAGRANGE variational equations.[7] In case of Mars, the semi-major axis a and likewise the orbit energy, $E = -\mu_{\mathrm{s}}/2a$, must be increased with a maximum rate. Accordingly, the sail's orbit-transversal acceleration component a_t needs to be maximized. As discussed previously, a solar sail provides a maximum a_t for cone angles $\alpha \approx 35$ deg. A clock angle $\alpha \neq 0$ results in a component of the sail force vector $\boldsymbol{F}_{\mathrm{SRP}}$ out of the orbital plane, creating an orbit normal acceleration component a_{h} and changing the inclination of the osculating orbit. Since the Mars orbit is only slightly inclined against the ecliptic ($\iota_{\mathrm{M}} = 1.85$ deg), the clock angle distribution is expected to depart only marginally from zero. Accordingly, the sail's steering strategy towards Mars is expected to follow these steering angle requirements over most parts of the trajectory, thus primarily flying with $\alpha \approx 35$ deg and $\delta \approx 0$ deg. The expected sail angular velocity for this strategy is small. The sail should provide a relatively constant α over time, thus the sail's $\boldsymbol{F}_{\mathrm{SRP}}$ direction must be steered likewise, while the sail is revoluting around the Sun on its outbound trajectory. In case of the Mars rendezvous mission, a control step size $\Delta t = 6$ hours is chosen for the trajectory optimization with both steering strategies, so that the NC is allowed to change the sail force vector direction (ITS strategy) or the control torques (CTS strategy) every 6 hours, respectively. The final accuracy limits at Mars are $\Delta r_{\mathrm{f,max}} = 100,000$ km and $\Delta v_{\mathrm{f,max}} = 100$ m/s. For both steering strategies, the sail starts from the Earth position with a hyperbolic excess energy of $0\ \mathrm{km^2/s^2}$. The launch window was chosen to be 30 days around the best preliminary found solution with a launch window size of the synodic period of Mars relative to Earth, $\Delta T_{\mathrm{syn}} = 780$ days. This increases the probability to find a global optimal solution due to a beneficial phasing between both planets during the transfer. For the CTS-controlled optimization, the allowed control torque limits are set to $T_{\mathrm{i,min}} = -10^{-3}$ Nm and $T_{\mathrm{i,max}} = 10^{-3}$ Nm about all body axes. The sail cone angle is limited to $\alpha < 90°$ and the maximum allowed angular velocity is set to $|\boldsymbol{\omega}_{\mathrm{max}}| = 20$ deg/day. In order to support the NC in finding a promising first solution, the initial conditions in terms of sail attitude are set to a cone angle $\alpha_{\mathrm{init}} = 35$ deg and s sail's angular velocity $\omega_{\mathrm{z,init}} = \omega_{\mathrm{orb,Earth}} = 0.986$ deg/day.

The second scenario is a Neptune flyby within a distance of less than 10^6 km from the planet. The Neptune orbit parameters are $a_{\mathrm{N}} = 30.07$ AU, $e_{\mathrm{N}} = 0.0086$ and $\iota_{\mathrm{N}} = 1.77$ deg. This mission requires multiple SPA maneuvers in close proximity to the Sun (< 0.3 AU), in order to gain enough

kinetic energy to reach Neptune in a reasonable flight time. Simply spiraling outwards to 30 AU would take several decades, even for mid- and long-term solar sail technologies. Therefore, the sail is not constantly spiraling outwards away from the Sun, as seen for the Mars transfer, but repeatedly approaches the Sun, gradually increasing its orbit eccentricity during the perihelion passage. After the last SPA, the sail finally reaches a hyperbolic escape trajectory towards Neptune. Throughout multiple revolutions around the Sun, the sail continuously decelerates with a maximum transversal acceleration component a_t against the direction of flight ($\alpha \approx 35$ deg, $\delta \approx 180$ deg), thus losing kinetic energy. This decreases the orbit perihelion and the sail spirals inwards towards the Sun. Close to perihelion, the sail changes its attitude in order to provide a maximum radial acceleration component a_r ($\alpha = 0$ deg, $\delta \approx 0$ deg). This force direction increases the orbit aphelion distance with maximum rate, by increasing the orbit's eccentricity and likewise the semi-major axis a. At this point during the SPA, the sail rapidly increases its orbit energy E. On the outbound leg after the perihelion passage, the sail again rotates its SRP force vector against the direction of flight (again $\alpha \approx 35$ deg, $\delta \approx 180$ deg), initializing the next deceleration-phase. Conclusively, each SPA requires a twofold maneuver strategy, as will be seen in the results below. These flight phases close to the orbit perihelion are identified to be the most challenging for a real AOCS, since each SPA consists of two maneuvers, which must be fulfilled within a few days. Ideally, the maneuvers take place within zero time, as will be seen for the ITS-controlled reference trajectory. This mission goal is identified to require the highest demands on attitude control for interplanetary solar sail missions. In case of the Neptune flyby mission, a control step size $\Delta t = 6$ hours is chosen for the trajectory optimization with both steering strategies. The final accuracy limit at Neptune is $\Delta r_{\mathrm{f,max}} = 10^6$ km and the maximum relative velocity is not restricted, due to the nature of the flyby problem. The sail starts from the same initial Earth-orbit as for the Mars transfer. The launch window is again chosen to be 30 days around the best preliminary found solution with a launch window size of the sidereal period of Earth, $\Delta T_{\mathrm{sid}} = 366$ days. For the CTS-controlled optimization, the allowed limits for the simulation constraints and the initial conditions are set as mentioned above for the Mars transfer.

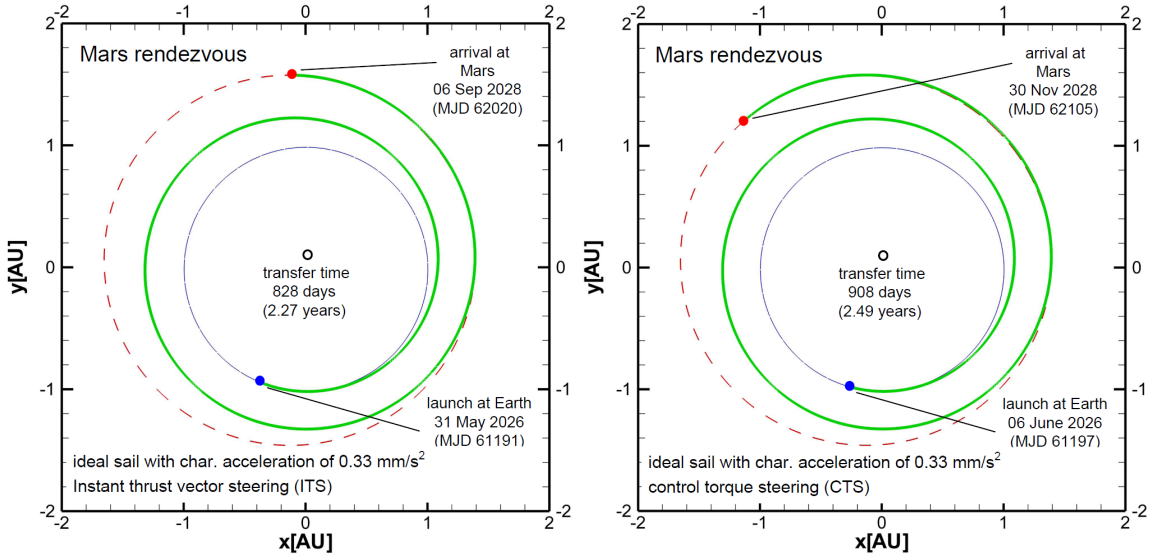

ITS strategy, TOF = 828 days

CTS strategy, TOF = 908 days

Figure 4: Mars rendezvous trajectories, obtained with the instant thrust vector steering strategy ITS (left) and control torque steering strategy CTS (right)

RESULTS

The resulting time-minimal transfer trajectories for the Mars scenario with the reference ITS control strategy and the new CTS control strategy are shown in Figure 4. The transfer time is 908 days for the CTS optimization in comparison to 828 days for the ITS-controlled reference mission trajectory and thus only 9.7 percent longer. The final target distance is $\Delta r_{\mathrm{f}} = 600$ km towards the planet's center for the ITS trajectory, with a final relative velocity of $\Delta v_{\mathrm{f}} = 100$ m/s. For the CTS trajectory, the final conditions are $\Delta r_{\mathrm{f}} = 1240$ km and $\Delta v_{\mathrm{f}} = 99$ m/s. This indicates a reasonably good minimum-time trajectory and underlines the capability of the new CTS strategy to find solutions close to the global optimum.

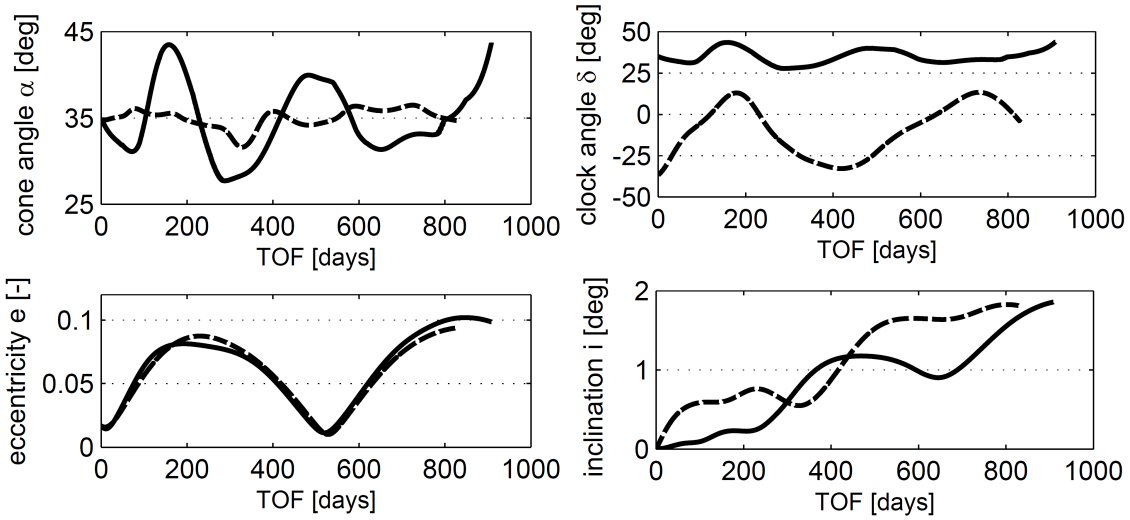

Figure 5: Mars rendezvous steering angles α (upper left) and δ (upper right), eccentricity (lower left) and inclination (lower right) over TOF, obtained with the instant thrust vector steering strategy ITS (dashed lines) and control torque steering strategy CTS (solid lines)

The steering angle distributions over TOF are shown in Figure 5 for both steering strategies, together with the osculating orbital elements eccentricity e and inclination ι. As expected, the cone angle always stays close to 35 deg, using the reference ITS steering, whereas its variation in case of the new CTS strategy is more dynamic. Since the reference ITS trajectory is faster, the sail angle steering with the new strategy is still suboptimal. However, the evolution of the transfer orbit is very similar for both steering strategies, as seen in the change of eccentricity. The final orbit inclination is reached 80 days later using CTS steering, which is identified as the main reason for the longer transfer time. During the transfer steered with the CTS strategy, the sail's angular velocity always stays within the margins $|\omega_{b_x}| < 0.85$ deg/day, $|\omega_{b_y}| < 1.13$ deg/day and $|\omega_{b_z}| < 1.05$ deg/day. This is plausible, since the sail must only compensate the changing relative attitude towards the sunlight vector, while spiraling in outbound direction. Starting at Earth, the sail has the same orbital angular velocity as Earth, $\omega_{\text{orb,Earth}} = 0.986$ deg/day, around the Sun, while Mars rotates with $\omega_{\text{orb,Mars}} = 0.529$ deg/day around the Sun. During the entire CTS-controlled transfer, the control torque magnitudes stay within the intervals $|T_{b_x}| < 1.6 \cdot 10^{-6}$ Nm, $|T_{b_y}| < 6.1 \cdot 10^{-6}$ Nm and $|T_{b_z}| < 2.1 \cdot 10^{-6}$ Nm. The control torque components T_i for the TOF interval [224,237] days are shown in Figure 6. The control torques change signs typically every first or second time step. A set of two changes of signs is regarded as one sub-maneuver on the smallest time-scale. In general,

two opposing torques of roughly the same magnitude combine to a rotation in one direction and subsequent braking, finalizing the maneuver and resulting in one distinct change of attitude.

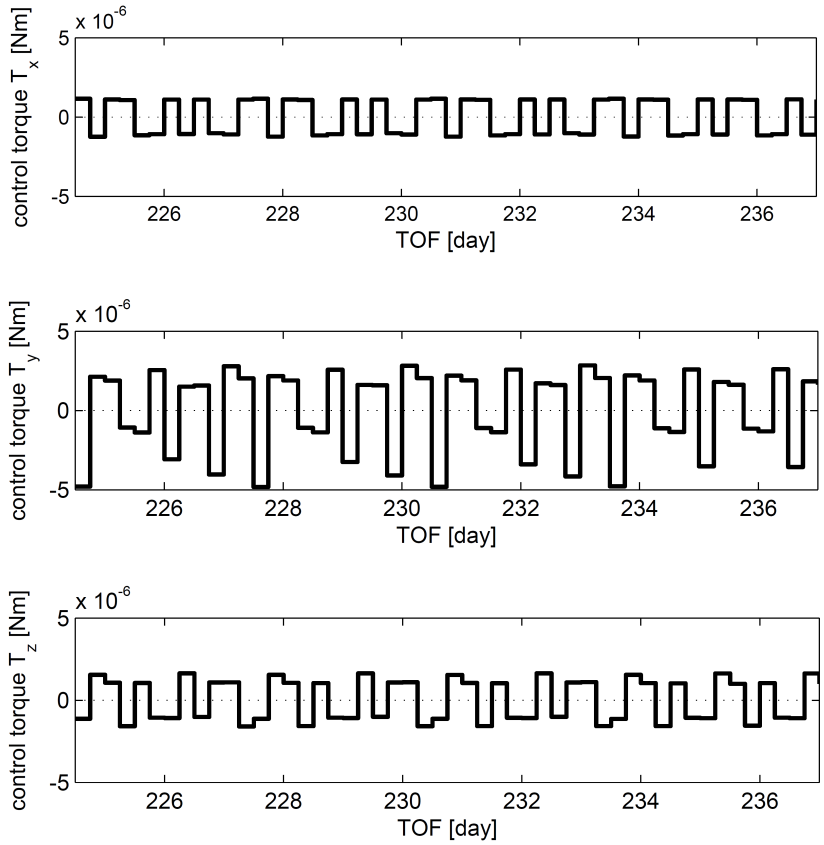

Figure 6: Mars rendezvous: variation of the control torque components over TOF interval [224,237] days using CTS

Since only minor changes in attitude are necessary during the Mars transfer, this control torque profile is plausible. The rate of change of the cone angle always stays below $|\Delta\alpha| = 0.1$ deg/step. This is in agreement with the analytical result of a sample single-axis rotation applied on the used sail configuration. For example, assuming a constant control torque component $T_{b_z} = 2 \cdot 10^{-6}$ Nm about the body z-axis for $\Delta t = 6$ hours, as typically seen in Figure 6, results in a change of rotation angle $\Delta\phi_z \approx 0.1$ deg/step. Here, the sail was initially not rotating ($\omega_z = 0$).

In case of the Neptune flyby, the obtained time-minimal transfer trajectories with both control strategies are shown in Figure 7. The transfer time is 7879 days (21.57 years) for the CTS optimization in comparison to 4765 days (13.05 years) for the ITS-controlled reference mission trajectory. The transfer time is 65 % longer. Although the result obtained with the CTS strategy is still far away from the optimal reference solution, a similar steering behaviour of the NC is clearly visible. The sail also fulfils three SPA maneuvers ($r < 0.3$ AU), as seen in the reference ITS trajectory. However, the attitude changes obtained with the new CTS strategy are slower than the ideal instant attitude changes within the ITS control strategy. Figure 8 shows the sail steering angle distributions for both steering strategies, together with the solar distance. The pictured TOF interval is [1000,2400] days for the ITS strategy and [2150,4600] days for the CTS strategy. Both intervals

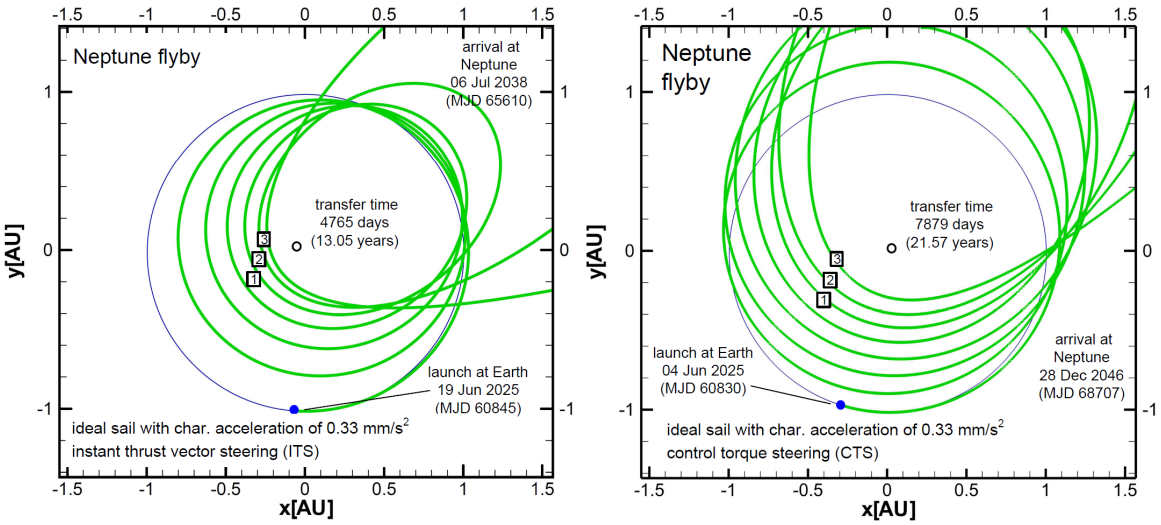

ITS strategy, TOF = 4765 days (13.05 years)

CTS strategy, TOF = 7879 days (21.57 years)

Figure 7: Neptune flyby trajectories, obtained with the instant thrust vector steering strategy ITS (left) and control torque steering strategy CTS (right)

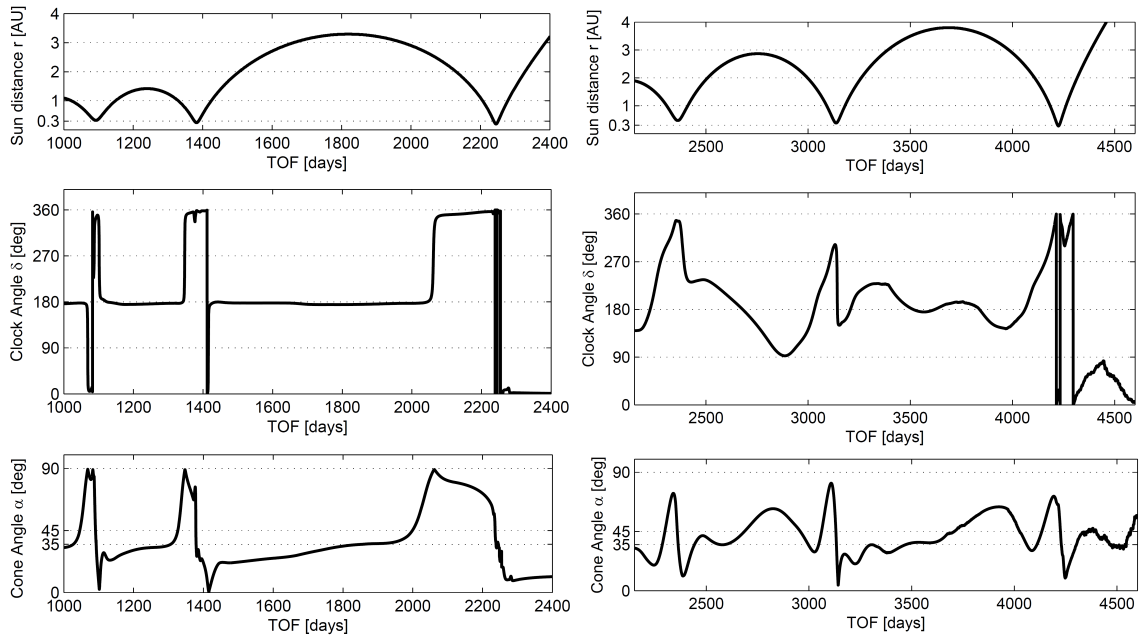

ITS strategy, TOF interval [1000,2400] days

CTS strategy, TOF interval [2150,4600] days

Figure 8: Neptune flyby: solar distance r and sail steering angles α and δ over TOF, obtained with ITS strategy (left) and CTS strategy (right)

cover all three SPA phases, respectively. Within far distance from the Sun, the NC commands steering angles $\alpha \approx 35$ deg and $\delta \approx 180$ deg, resulting in a maximum transversal acceleration component a_t against the direction of flight. Shortly before the perihelion passage, the sail rotates

to $\alpha \approx 0$ deg and $\delta \approx 0$ deg, providing a maximum radial acceleration component a_r. After the perihelion passage, the sail rotates again towards a maximum-negative a_t.

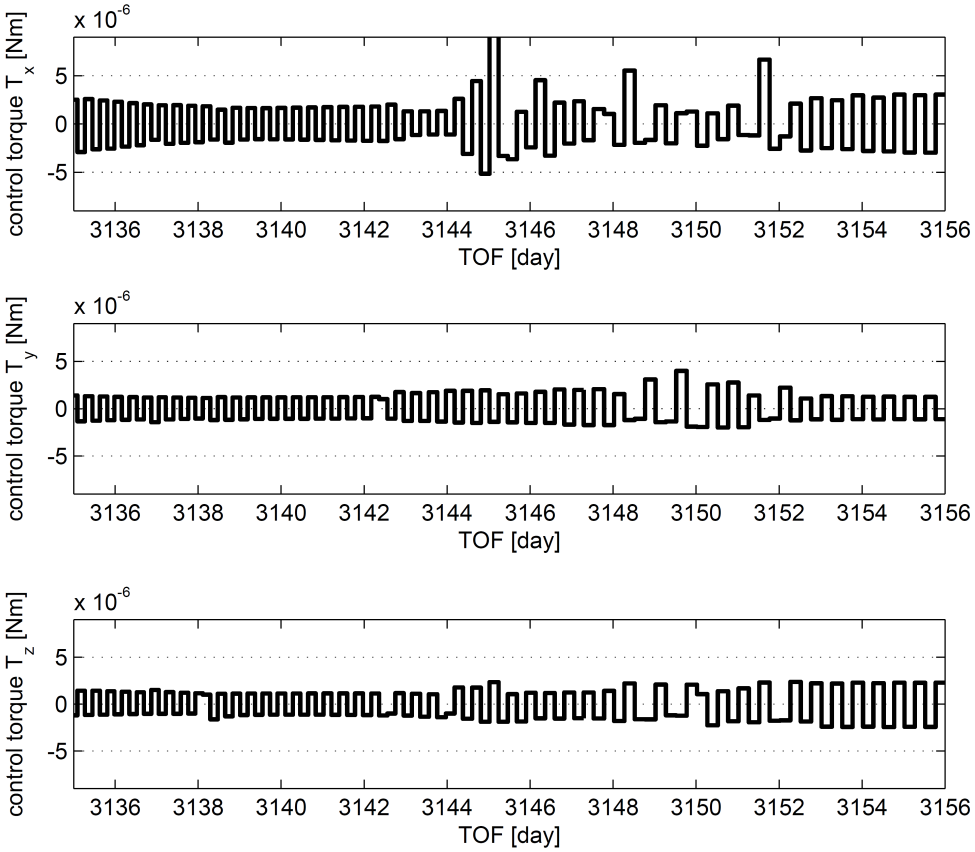

Figure 9: Neptune flyby: variation of the control torque components over TOF interval [3135,3156] days using CTS

This twofold steering behaviour is characteristic for SPAs. As visible in Figure 8, the changes in the sail steering angles are more distinct in case of the reference ITS strategy, since the sail is allowed to rotate its SRP froce vector direction instantaneously. However, the necessary steering strategy is very complex and the NC probably needs to be trained longer using multiple subsequent refine-runs to approach the ideal steering case. During the entire transfer, the control torque magnitudes stay within the intervals $|T_{b_x}| < 2.5 \cdot 10^{-5}$ Nm, $|T_{b_y}| < 3.1 \cdot 10^{-5}$ Nm and $|T_{b_z}| < 3.3 \cdot 10^{-5}$ Nm. It can be noticed that the NC is not using the full bandwidth of allowed control torques. The given limits were $T_{\text{i,min}} = -10^{-3}$ Nm and $T_{\text{i,max}} = 10^{-3}$ Nm about all body axes, as stated above. This may refer to a suboptimal processing of the NC input and output values and is subject to further investigation. The control torque components T_i for the TOF interval [3135,3156] days are shown in Figure 9. Since the control step size was $\Delta t = 6$ hours, the full torque profile can not be visualized. During the CTS-controlled transfer, the sail's angular velocity always stays within the margins $|\omega_{b_x}| < 13.2$ deg/day, $|\omega_{b_y}| < 6.9$ deg/day and $|\omega_{b_z}| < 6.5$ deg/day. The values are quite close to the predefined simulation constraint of $|\boldsymbol{\omega}_{\text{max}}| = 20$ deg/day, thus releasing this constraint may result in faster transfers in case of the Neptune flyby.

CONCLUSIONS

The novel method presented in this paper provides a new approach to the low-thrust trajectory optimization problem for solar sails. A new steering strategy, controlling the solar sail with generic torques applied about the spacecraft body axes, was built into the low-thrust trajectory optimization software *InTrance*. The interplanetary trajectory results obtained with the new 'control torque steering' strategy were in reasonable agreement with the reference solutions, steering the sail by instant changes of the sail force vector. The resulting transfer time to Mars was only 9.7 percent longer compared to the obtained 'instant thrust vector steering' solution. It showed the same final accuracy in terms of target distance and relative velocity. In case of the Neptune flyby, the neurocontroller could not reach the time-optimal reference solution, but showed a similar steering behaviour using multiple solar photonic assist maneuvers around the Sun. The required control torque magnitudes in order to steer the employed 160-m, 450-kg square solar sail during the selected missions were investigated. In case of Mars, they resulted to range within the interval $[-0.006 \cdot 10^{-3}, 0.006 \cdot 10^{-3}]$ Nm. For the Neptune mission, the magnitudes were $[-0.04 \cdot 10^{-3}, 0.04 \cdot 10^{-3}]$ Nm. However, the neurocontroller did not use the full range of allowed control torques, $[-1.0 \cdot 10^{-3}, 1.0 \cdot 10^{-3}]$ Nm, especially in case of the Neptune mission. Compared to the 'instant thrust vector steering' strategy, this caused delays in the sail-angle steering that can not be solely justified by the modelled mass moments of inertia of the sail. Since the necessary steering strategy is very complex, the neurocontroller most likely needs to be trained longer using multiple subsequent refine-runs to approach the ideal instant steering case. At the end of this investigation, the results demonstrate the general capability of the new steering method to find near-optimal trajectory solutions to this kind of problem. Using the implemented attitude dynamics model, the neurocontroller provides reasonable and reproducible steering strategies for solar sails in case of a Mars transfer that are close to the existing 'instant thrust vector steering' strategy in *InTrance*. However, in case of the investigated Neptune flyby, further investigations are necessary due to the complexity of the optimal steering strategy.

ACKNOWLEDGEMENT

This study was completed when Andreas Borggräfe was a diploma candidate at the Institute of Flight System Dynamics of the RWTH Aachen University, Germany.

APPENDIX A: ROTATING POLAR REFERENCE FRAME

The translational equations of motion are expressed in terms of the heliocentric rotating polar ecliptic reference frame $\mathcal{E} : (\vec{e}_r, \vec{e}_\varphi, \vec{e}_\theta)$, an orthogonal right-handed coordinate frame. It is defined according to Figure 10.

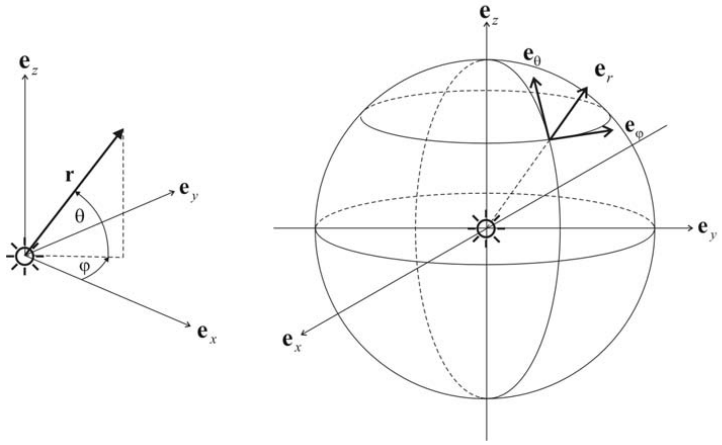

Figure 10: Ecliptic reference frame, taken from[3]

$\vec{e}_r$ points always along the Sun-spacecraft line, $\vec{e}_\theta$ lies in the $(\vec{e}_r, \vec{e}_z)$ plane and points along the direction of increasing θ, and $\vec{e}_\varphi$ completes the right-handed coordinate frame $(\vec{e}_r \times \vec{e}_\varphi = \vec{e}_\theta)$.

APPENDIX B: ORBIT REFERENCE FRAME

The orbit reference frame is an orbit-based orthogonal right-handed polar coordinate frame $\mathcal{O} = (\vec{e}_r, \vec{e}_t, \vec{e}_h)$. According to Figure 11, $\vec{e}_r$ points always along the Sun-spacecraft line, $\vec{e}_h$ is the orbit plane normal (pointing along the spacecraft's orbital angular momentum vector) and $\vec{e}_t$ completes the right-handed coordinate system.

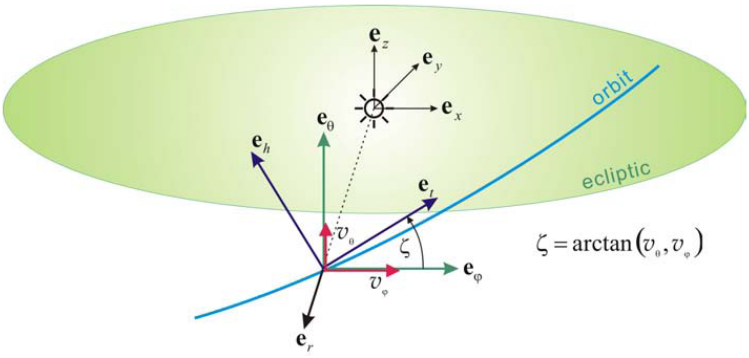

Figure 11: Orbit reference frame, taken from[3]

APPENDIX C: QUATERNION PRODUCT

In order to use quaternions for rotational operations, the product of two quaternions or HAMILTON product is defined as follows.[10] Given two quaternions $\bar{s} = (s_1, s_2, s_3, s_4)^{\mathrm{T}}$ and $\bar{t} = (t_1, t_2, t_3, t_4)^{\mathrm{T}}$, each representing an arbitrary attitude of a body frame $\mathcal{B}$ relative to a chosen reference frame $\mathcal{I}$. The following quaternion product returns the quaternion $\bar{q} = (q_1, q_2, q_3, q_4)^{\mathrm{T}}$ that represents the final attitude*

$$\bar{q} = \bar{s} \otimes \bar{t} = \begin{pmatrix} s_4 \cdot \vec{t} + t_4 \cdot \vec{s} + \vec{s} \times \vec{t} \\ s_4 \cdot t_4 - \vec{s} \cdot \vec{t} \end{pmatrix} \tag{5}$$

REFERENCES

[1] M. Leipold, H. Fichtner, B. Heber, P. Groepper, S. Lascar, F. Burger, M. Eiden, T. Niederstadt, C. Sickinger, L. Herbeck, B. Dachwald, and W. Seboldt, "Heliopause Explorer - A Sailcraft Mission to the Outer Boundaries of the Solar System," *Acta Astronautica*, Vol. 59, No. 8-11, 2005, pp. 785–796.

[2] B. Wie and D. Murphy, "AOCS Design for a 160-M,450-KG Solar Sail Spacecraft of the Solar Polar Imager," *6th International ESA Conference on Guidance, Navigation and Control Systems, held 17-20 October 2005 in Loutraki, Greece. Edited by D. Danesy. ESA SP-606. European Space Agency*, 2006.

[3] B. Dachwald, *Low-Thrust Trajectory Optimization and Interplanetary Mission Analysis Using Evolutionary Neurocontrol*. Doctoral Thesis, Fakultät für Luft- und Raumfahrttechnik, Institut für Raumfahrttechnik,Universität der Bundeswehr München, Munich, Germany, 2004.

[4] C. R. McInnes, *Solar Sailing: Technology, Dynamics and Mission Applications*. Springer-Praxis Series in Space Science and Technology, 2nd ed., 2004.

[5] A. Borggräfe, *Analysis of Interplanetary Solar Sail Trajectories with Attitude Dynamics*. Diploma Thesis, Institute of Flight System Dynamics, RWTH Aachen University, Aachen, Germany, 2011.

[6] B. Dachwald, "Optimal Solar-Sail Trajectories for Missions to the Outer Solar System," *Journal of Guidance, Control, and Dynamics*, Vol. 28, No. 6, 2005.

[7] R. H. Battin, *An Introduction to the Mathematics and Methods of Astrodynamics*. AIAA, 1987.

[8] B. Dachwald, "Optimization of Interplanetary Solar Sailcraft Trajectories Using Evolutionary Neurocontrol," *Journal of Guidance, Control, and Dynamics*, Vol. 27, No. 1, 2004.

[9] B. Dachwald, A. Ohndorf, and B. Wie, "Solar Sail Trajectory Optimization for the Solar Polar Imager (SPI) Mission," *AIAA/AAS Astrodynamics Specialist Conference and Exhibit, 2006*.

[10] M. Sidi, *Spacecraft Dynamics and Control: A Practical Engineering Approach*. Cambridge University Press, 2000.

*Note that the '$\otimes$' sign is used between the factors to distinguish the quaternion product from other vector multiplication forms.